

Optical Anisotropy and Dimple Formation on Films Formed after Drying of Gelatinized Starch Solution Droplets

Subhadip Ghosh and Arun Roy*

Cite This: *ACS Omega* 2023, 8, 19994–20003

Read Online

ACCESS |



Metrics & More

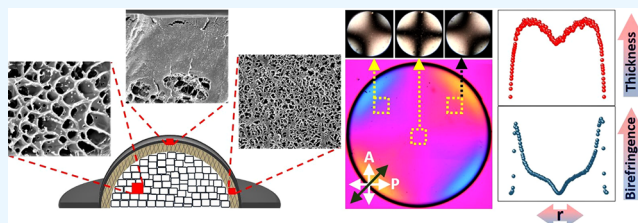


Article Recommendations



Supporting Information

ABSTRACT: We study the microstructures in the drying droplets of gelatinized starch solutions on a flat substrate. Cryogenic scanning electron microscopy studies on the vertical cross-section of these drying droplets for the first time reveal a relatively thinner solid elastic crust of uniform thickness at the free surface, an intermediate mesh region below the crust, and an inner core of a cellular network structure made of starch nanoparticles. We find that the deposited circular films formed after drying are birefringent and azimuthally symmetric with a dimple at their center. We propose that the dimple formation in our sample occurs due to the evaporation-induced stress on the gel network structure in the drying droplet. The polarizing optical microscopic studies show that these films are optically uniaxial at their center and increasingly biaxial away from the center.



INTRODUCTION

The study of various properties of the solute films formed upon drying of solution droplets cast on a flat substrate has been an active field of research during the last two decades. The solution droplets of various solutes such as polymers,^{1–3} DNA,^{4,5} nanotubes,^{6–9} nanorods,^{10,11} liquid crystals,^{12,13} colloids,^{14–17} surfactants,¹⁸ salts,^{19,20} and biological materials^{21–23} have been used for this purpose. The most spectacular phenomenon found after the drying of such a dilute solution droplet is the coffee ring effect.^{14,15} In this phenomenon, a circular stain is found to form due to the outward capillary flow of solute particles toward the pinned edge of the droplet upon evaporation of the solvent. The deposited film formed in this way shows the highest thickness near its edge. However, the pattern of deposited film depends on the properties of solute particles,²⁴ the ambient conditions,²⁵ and the properties of substrates.^{25–27} Interestingly, self-assembled structures of solute ingredients have also been observed in some cases which make the deposited thin films birefringent.^{4,8,9,12,28}

Kajiya et al. studied this coffee ring effect as a function of the concentration of a polymeric solution.³ They found that the mismatch in the thickness of the dried film at its rim and the center reduces with increasing the initial polymer concentration, and the film became almost flat at a certain concentration. Further increase of the solute concentration again started to produce a dimple at the center of the dried film which became deeper on increasing the solute concentration. The mechanism of this dimple formation in the films for higher solute concentrations is found to be different from that of lower solute concentrations. It has been proposed that this dimple formation in the higher concentration regime is driven by the buckling of a crust formed at the free surface of a

droplet during its drying.^{3,29–31} However, detailed studies on the microstructure inside these drying droplets have not yet been performed. A few models on crust formation at the free surface of different solution droplets have also been proposed.^{32,33}

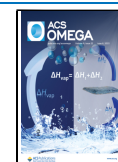
Here, we have studied the properties of the biodegradable films formed on drying droplets of gelatinized starch solutions cast on a flat plastic substrate. Starch, the most abundant and consumable carbohydrate, is the source of large polysaccharides found in nature. Starch naturally occurs in the form of grains and is made of amylose and amylopectin which are generally linear and branched polymers, respectively. The starch grains on heating in excess water swell and rupture irreversibly by imbibing water above a certain temperature. This process allows the starch polysaccharides to disperse in water and is known as the gelatinization of starch.³⁴ The gelatinized starch solutions cast on a flat substrate produce transparent films after drying.^{35–37} In recent years, starch-based bioplastics have attracted much attention as a replacement for synthetic polymer films in plastic industries due to their biodegradable properties.³⁸

We report detailed cryogenic scanning electron microscopy studies on the vertical cross-section of drying gelatinized starch solution droplets to investigate the microstructure inside them.

Received: March 31, 2023

Accepted: May 5, 2023

Published: May 22, 2023



The circular starch films formed upon complete drying are found to be azimuthally symmetric with a dimple at their center. Using polarized optical microscopy and conoscopy studies, we find that the films are optically uniaxial at the center with an optic axis normal to the film whereas they are increasingly biaxial away from the center. Based on our experimental results, we propose the possible origin of the formation of the dimple as well as the birefringence in the films.

■ EXPERIMENTAL METHODS

Preparation of Starch Solutions and Films. The starch grains were extracted from potatoes procured locally from a market. A beaker containing starch grains dispersed in water was closed tightly by using aluminum foil and kept at 90 °C for 1.5 h with continuous stirring of the sample using a magnetic stirrer. At this temperature, the starch grains become completely gelatinized. The cooled sample was then homogenized using an ultrasonic probe sonicator (QSONICA Q700). A 17 mL aliquot of the starch solution was taken in a 20 mL glass bowl and sonicated in pulsed mode (2 s on/4 s off) for 10 min with 40% amplitude of vibration using a 6 mm diameter tip. The sonicated starch solution was then cooled to room temperature by keeping it in a water bath for 5 min. Five different gelatinized starch solutions were prepared with concentrations of 10.8, 9.5, 8.0, 6.5, and 5.0 wt %, respectively, for our experimental studies. These solutions were dropcasted on a flat plastic substrates by using a micropipette. The droplets, upon complete drying at room temperature and ambient humidity, produce starch films on the substrate. The flat plastic substrates were used as the films produced can be easily detached from the substrate for further studies.

Weight Measurement during Drying. The weight loss during the drying of a starch solution droplet was measured using a quartz crystal microbalance with precision of 10^{-4} g. For each experiment, 150 μ L of starch solution was dropcasted on the flat surface of a plastic petridish using a micropipette. This droplet was then allowed to dry in air at room temperature (about 25 °C) and humidity in the range 53%–55%.

Polarizing Optical Microscopy (POM) and UV–Visible Spectroscopy. Both the conoscopic and orthoscopic polarizing optical microscopy (POM) studies of starch films were performed by using an Olympus BX50 polarizing optical microscope. The UV–visible transmission spectroscopy studies of starch films were performed by using a Lamda 35 PerkinElmer spectrophotometer.

Linear Birefringence Measurement Setup. A customized experimental setup using a photoelastic modulator (PEM) was used to measure the retardation of the circular starch film along its diameter (see the [Supporting Information](#) for details). The thickness profile of the film was measured by cutting it along the same diameter after the retardation measurement and taking the cross-sectional image by using a microscope (Olympus BX50) attached with a digital camera (Canon EOS 80D). The digital image processing software (imageJ, NIH) was used to obtain the thickness profiles of the films. The linear birefringence profile of the film was calculated from the ratio of the measured optical path difference and the corresponding thickness.

Cryo-Scanning Electron Microscopy (Cryo-SEM). The cryo-SEM studies on the starch solution droplets were

performed by using a Carl Zeiss (Ultra Plus model) system (see the [Supporting Information](#) for details).

X-ray Diffraction (XRD). A DY 1042-Empyrean (PANalytical) X-ray diffractometer with PIXcel 3D detector was used for acquiring the XRD profiles of the samples using Cu K_{α} radiation of wavelength 1.54 Å. The samples were kept on a flat silicon stage of the diffractometer to acquire their XRD profiles, and the measurements were performed in the grazing angle of incidence of the X-ray beam. The silicon stage gives a flat XRD profile which does not interfere with the sample profiles.

■ RESULTS

The native potato starch grains are spherical or elliptical in shape and about 10 to 60 μ m in size. The native starch grains are semicrystalline in nature and possess birefringent properties. The potato starch grains upon heating in excess water gelatinize in the temperature range from 60 to 75 °C. In this process, starch grains lose their crystalline and birefringent properties.^{39,40} The resulting gelatinized starch solution is inhomogeneous due to the presence of so-called “ghost” structures of grains and the entangled starch biopolymers.^{41,42} A homogeneous starch solution can be prepared by sonicating the gelatinized sample. Probe sonication of this sample breaks the starch biopolymers into nanoparticles and gives rise to a homogeneous, transparent, and less viscous starch solution. These starch solutions with various initial starch concentrations were dropcasted on a plastic substrate, and circular transparent potato starch films were formed upon drying in ambient conditions.

The drying dynamics of a starch droplet on a plastic substrate were studied as a function of time after its dropcasting. [Figure 1a](#) shows the images of a 150 μ L droplet with 5.0 wt % starch concentration at different time intervals of its drying. Initially, the droplet dries with its edge pinned to the substrate. After about 170 min, the droplet edge starts to recede toward the center with the deposition of a peripheral film from the initial pinned edge of the droplet. Further drying reduces the effective diameter of the central spherical cap of the sample. The time variation of the diameter of the circular edge of the droplet cap normalized by the initial diameter of the droplet is shown in [Figure 1a](#). Initially, this normalized diameter remains constant and starts to decrease after about 170 min. The complete drying of this droplet gives rise to a circular starch film with a diameter same as that of the initial droplet.

The variation of the weight of this drying droplet with time is shown in [Figure 1b](#). Initially, the weight of the droplet decreases linearly due to the constant rate of evaporation of water which was about 0.40 mg/min. The rate of weight loss starts to decrease gradually after about 170 min until the complete drying of the droplet. Therefore, we find that the decrease in the rate of weight loss is correlated with the receding of the droplet edge. The sample has negligible weight loss after its complete drying.

Similar dynamics were also found for other starch solution droplets with the same initial volume but different starch concentrations. The time variation of weight for a 150 μ L starch solution droplet with a 9.5 wt % initial starch concentration is shown in [Figure S3](#) of the [Supporting Information](#). Initially, the weight loss rate was constant at about 0.36 mg/min, and the rate subsequently started to decrease with the receding of the droplet edge which occurred

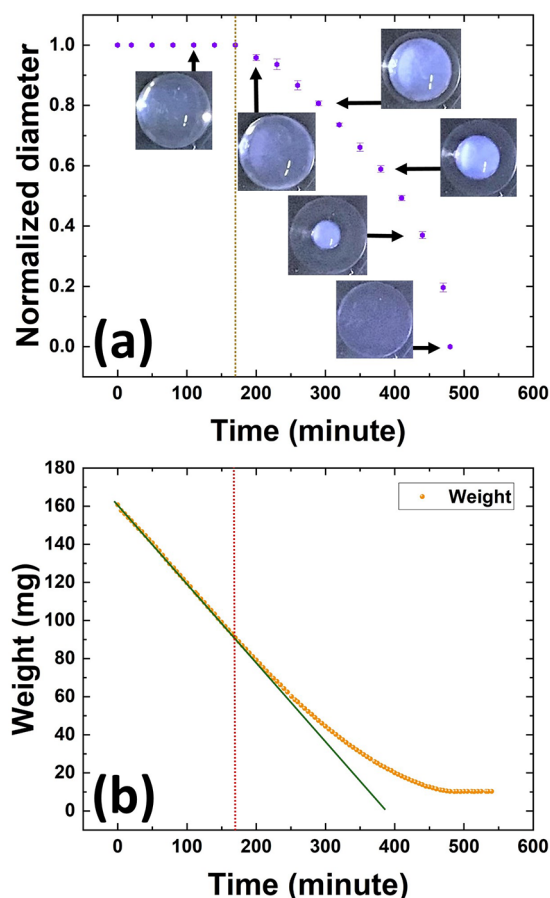


Figure 1. (a) The variation of normalized diameter of a 150 μL starch solution droplet with 5.0 wt % starch concentration during its drying. The images show the sample corresponding to some of the data points as indicated. (b) The variation of weight during its drying. The straight line (green) shows the initial linear variation of the weight with a 0.40 mg/min weight loss rate.

more than 100 min from its dropcasting. But our SEM studies reveal that a gel network forms in the droplet of this concentration within about 10 min of its dropcasting. Therefore, the decrease in the weight loss rate is independent of sol–gel transition but depends on the drying dynamics of the droplets.

The starch solution droplets after drying produce circular films on the substrate. These circular films have azimuthal symmetry with a radial variation of their thickness. Figure 2a shows the thickness profiles along the diameter of starch films formed after the drying of different volumes of droplets with a same initial starch concentration of 9.5 wt %. It is found that all these profiles show a sharp increase near the edge of the films and a dimple at their center, giving rise to an “M-shaped” thickness profile. The films have a maximum thickness h_{max} and radius r_0 depending on the initial volume of the droplets. The normalized thickness profiles (h/h_{max}) of these films when plotted with their normalized radial distance (r/r_0) collapse to a single curve as shown in Figure 2b. Therefore, the scaled thickness profile (h/h_{max}) is a function of only the scaled radial distance (r/r_0) when other experimental parameters remain same.

Figure 2c depicts the thickness profiles of starch films formed from the same volume of droplets (300 μL) but with different initial starch concentrations. The normalized thick-

ness profiles (h/h_{max}) as a function of normalized radial distance (r/r_0) of the data shown in Figure 2c are plotted in Figure 2d. The dimple at the center of the film formed from the droplet with 10.8 wt % initial starch concentration is deeper and wider compared to that of the film formed from the droplet with 5.0 wt % initial starch concentration. Therefore, the variation of (h/h_{max}) with (r/r_0) of the films depends on the initial starch concentration of the droplets.

The dried starch films are transparent in visible light (see Figure S4 in the Supporting Information). The XRD profiles of potato starch grains and starch films as shown in Figure 3 were measured to determine their crystalline structure. The profiles exhibit peaks on top of a broad amorphous hump. This indicates that the samples are semicrystalline in nature. The peak positions in the XRD profile of native starch grains agree with those found for the potato starch grains having a B-type of crystal polymorph with hexagonal lattice structure.^{43–46} The similarity of the diffraction profiles shown in Figure 3 indicates that the film also has a B-type of crystal polymorph.

The circular starch films are found to be linearly birefringent. The deposited starch film becomes birefringent after drying the droplet though the gelatinized starch solution is optically isotropic. Figure 4a shows the POM texture of a starch film formed after drying a 10 μL droplet with a 10.8 wt % starch concentration. The film between crossed polarizers appears gray-white which implies that the retardation introduced by the film is in the first order of the Levy chart. The black brushes of the Maltese cross along the pass axis of polarizers divide the whole circular film into four quadrants and remain invariant on rotating the sample on the microscope stage. These observations indicate that the principal axes of index ellipse on the film are along the radial and azimuthal directions, respectively. The POM studies using a λ -plate (530 nm) were performed to determine the orientation of the major axis. The introduction of the λ -plate with the slow axis at an angle of 45° with respect to the polarizer changes the color of the first and third quadrants to yellow, whereas the second and fourth quadrants become blue as shown in Figure 4b. These colors belong to the first and second order of the Levy chart, respectively. Therefore, the effective addition and subtraction of the optical path differences occur in the blue and yellow colored quadrants, respectively. These observations imply that the major and minor axes of the index ellipse on the sample are along the azimuthal and the radial directions of the film, respectively.

The center of the film between crossed polarizers appears dark which implies that this region is either optically isotropic or uniaxial with an optic axis along the normal to the film. The conoscopic studies were performed to determine the nature of the optical anisotropy of the dried starch films. Figure 5a shows the conoscopic figures at the center ($r = 0$) and at $r = 3$ mm of a starch film of diameter about 16 mm formed after drying a 600 μL droplet of concentration 9.5 wt %. The bottom row in Figure 5a shows the conoscopic figures at the center of the film for three different orientations of the sample on the microscope rotation stage in the absence and presence of a λ -plate in the optical path. The intersection point of the crossed isogyres parallel to the polarizers in the conoscopic figures without a λ -plate is always at the center of the field of view. This observation confirms the optical uniaxiality of the central region with an optic axis normal to the film.⁴⁷ The insertion of the λ -plate into the optical path changed the color of the first and third quadrants to yellow, whereas the second

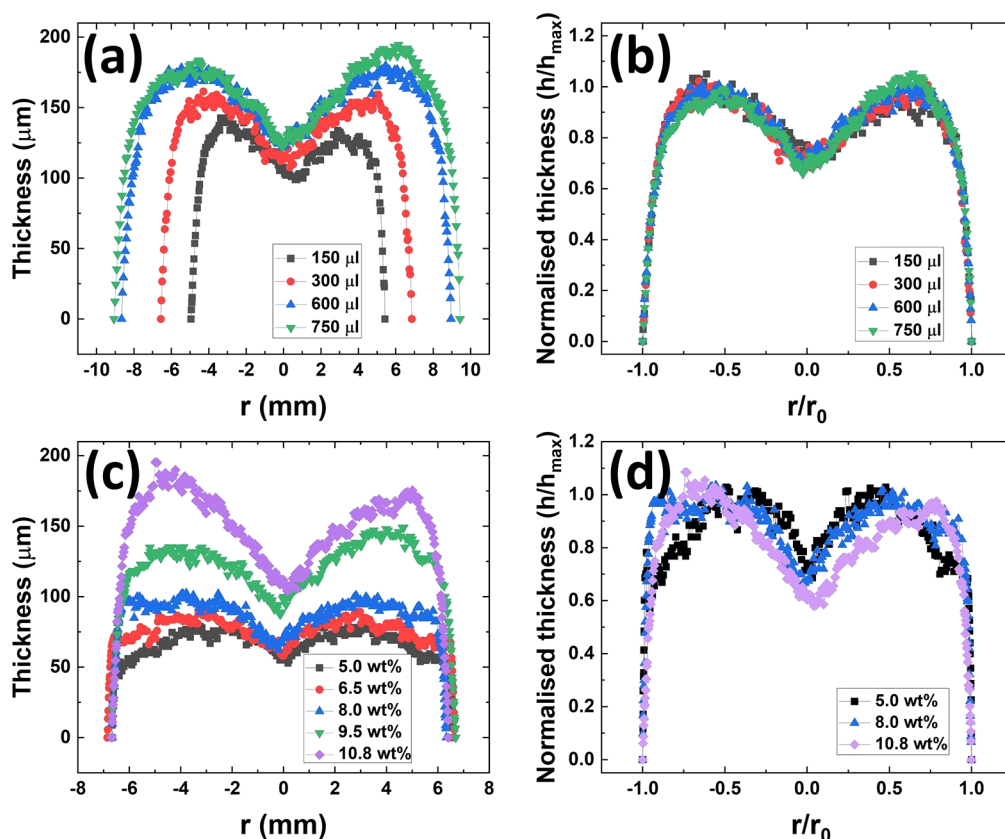


Figure 2. (a) The thickness profiles along the diameter of starch films formed from different volume of starch solution droplets with 9.5 wt % initial starch concentration. (b) The corresponding normalized thickness profiles as a function of the normalized radial distance. (c) The thickness profiles along the diameter of starch films formed from 300 μL droplets with different starch concentrations. (d) The corresponding normalized thickness profiles as a function of the normalized radial distance.

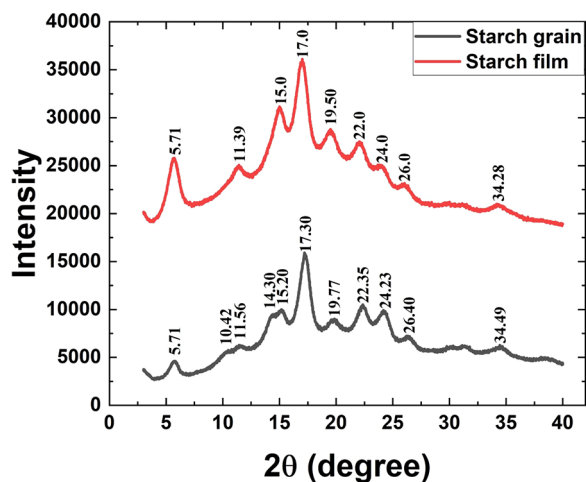


Figure 3. XRD intensity profiles of native potato starch grains and the film formed from a 600 μL droplet with 9.5 wt % starch concentration.

and fourth quadrants became blue (see bottom row of Figure 5a). It can be concluded from these observations that the sign of the birefringence at the central region of the film is negative. Hence, the conoscopic studies confirm that the index ellipsoid at the center of the film has a uniaxial oblate shape.

The top row in Figure 5a shows the conoscopic figures at $r = 3$ mm of the film for three different orientations of the sample on the microscope rotation stage. On rotating the film by 360°

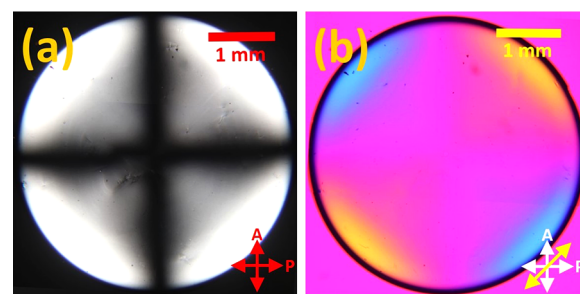


Figure 4. POM images of the starch film (a) between crossed polarizers and (b) after inserting of a λ -plate with the slow axis at an angle of 45° with respect to the polarizer.

on the microscope stage, the conoscopic figures at this location show that the isogyres become crossed at four distinct positions with a difference of 90° . At $\pm 45^\circ$ with respect to a crossed position, the isogyres separate and become hyperbolic (see the top row of Figure 5a) which indicates the optical biaxiality of the film at this position.⁴⁷ These hyperbolic isogyres containing the poles of the two optic axes at their apex are centered at the middle of the field of view. Further, the intersection point of the isogyres at crossed positions also lies at the center of the field of view. These observations indicate that one of the principal axes of the index ellipsoid with the refractive index denoted as α and the optic plane are perpendicular to the film at this biaxial region. The orthoscopic studies as discussed above confirm that the other principal axes with indices denoted as γ and β on the plane of

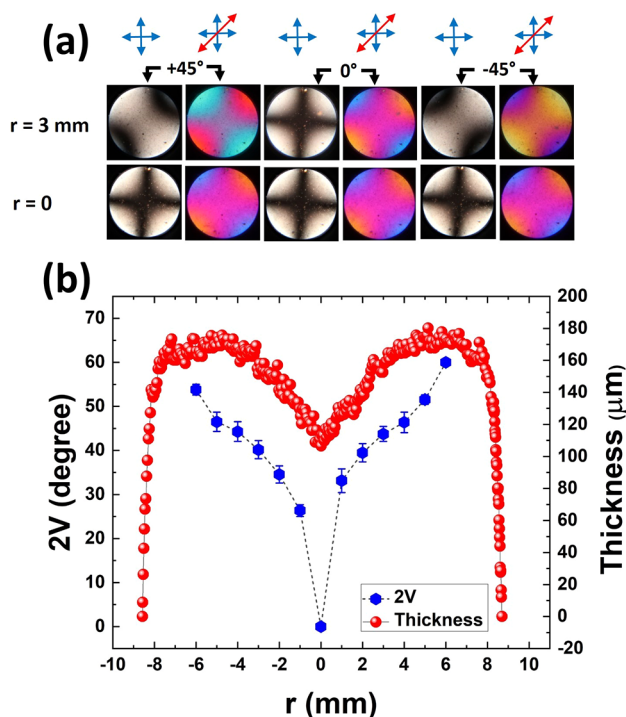


Figure 5. (a) The conoscopic figures of starch film at $r = 0$ (bottom row) and at $r = 3$ mm (top row) for three different orientations of the sample on a microscope stage with and without the λ -plate. The angles 0° and $\pm 45^\circ$ refer to the orientation of the optic plane with respect to the polarizer in the biaxial region of the sample. (b) The variation of the acute axial angle $2V$ along the radial direction of a film formed after drying of a droplet ($600 \mu\text{L}$, 9.5 wt %). The thickness profile of the film is also shown in this figure.

the film are along the azimuthal and the radial directions, respectively. The conoscopic studies after inserting a λ -plate (530 nm) in the optical path were performed to determine the order of the principal indices α , β , and γ at the biaxial region of the film. The insertion of the λ -plate at a $+45^\circ$ orientation of the optic plane to the polarizer changed the color in the region between the uncrossed isogyres to blue, whereas it became yellow at a -45° orientation of the optic plane as shown in Figure 5a (top row). Therefore, from these observations, it can be concluded that the film in its biaxial region is optically negative, and α is the minor principal index. So the optic plane containing the major principal index γ and minor principal index α lies along the azimuthal direction and perpendicular to the film. The intermediate principal axis with the index β is along the radial direction of the film.

The film is uniaxial at its center and becomes increasingly biaxial along the radially outward direction. The acute axial angle $2V$ between the two optic axes can be measured from the conoscopic studies (see the Supporting Information for the detailed procedure). The variation of the angle $2V$ along the diameter of a starch film formed from a $600 \mu\text{L}$ solution droplet with 9.5 wt % initial starch concentration is shown in Figure 5b. The angle $2V$ is zero at the uniaxial center, and it increases monotonically toward the edge of the film. The hyperbolic isogyres go out of the field of view for $r > 6$ mm of the film (see Figure S7 in the Supporting Information), and the measurement of the axial angle was not possible.

The anisotropic optical properties of these starch films arise due to the orientational order of the starch biopolymers that

developed during drying. Therefore, measuring the linear birefringence along the radial direction of starch films provides valuable insight into the structure of these films. Figure 6a

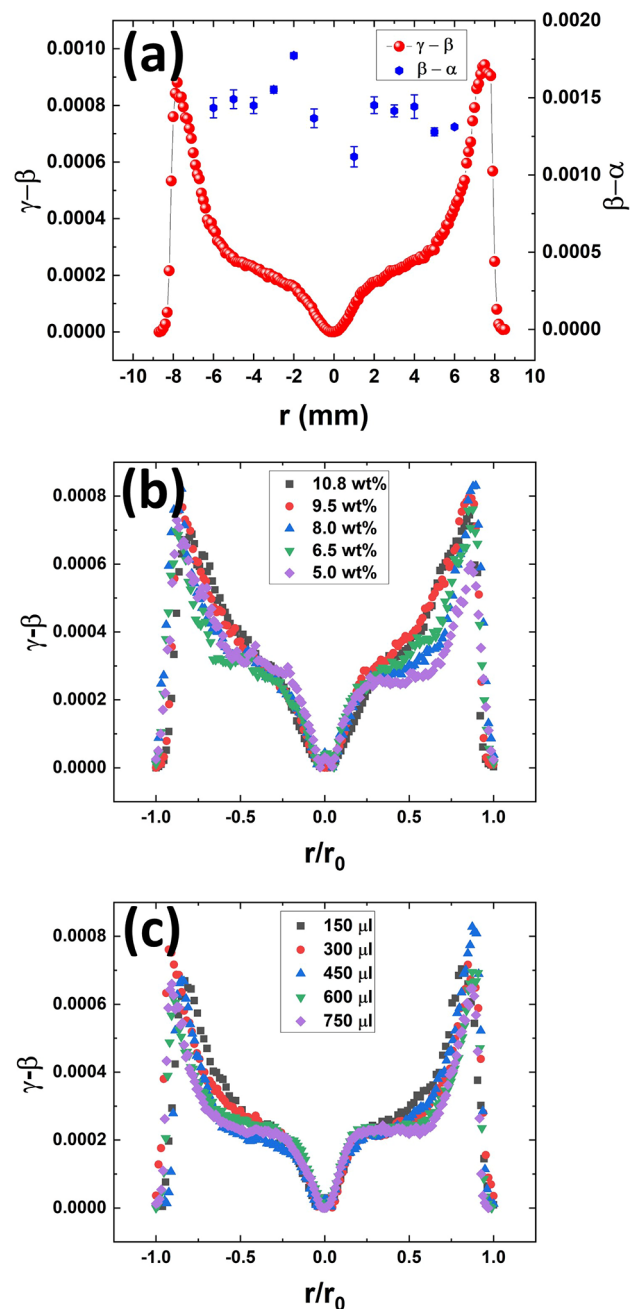


Figure 6. (a) The variation of $(\gamma - \beta)$ and $(\beta - \alpha)$ along the diameter of a starch film obtained from a droplet ($600 \mu\text{L}$, 9.5 wt %). The variation of $(\gamma - \beta)$ as a function of normalized radial distance on starch films formed from (b) $300 \mu\text{L}$ droplets with different starch concentrations and (c) different volumes of droplets with 6.5 wt % starch concentration.

shows the variation of effective linear birefringence $(\gamma - \beta)$ along the diameter of a starch film formed after drying a $600 \mu\text{L}$ droplet of concentration 9.5 wt % measured by using the PEM technique. The birefringence profile along the radial direction from the center to the edge of the film can be divided into three regions with three different slopes. The measured birefringence at the center of the film is zero due to its uniaxial

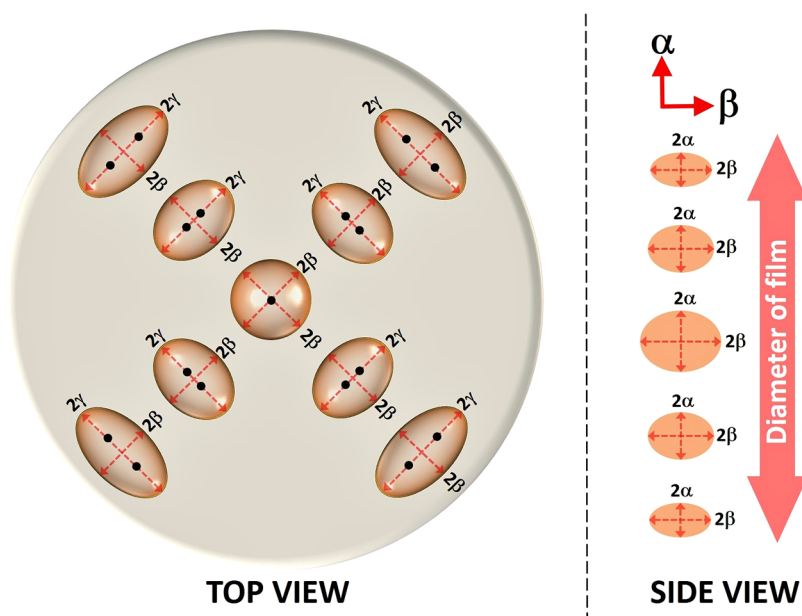


Figure 7. (Left) The schematic representation of the index ellipsoids at different positions along the diameter of a starch film. (Right) The variation of index ellipse in the α - β plane along the diameter of the film.

nature. Initially, the birefringence increases rapidly along the radially outward direction from the center. Then it increases with a relatively lower slope and again increases rapidly to the maximum value near the edge of the film.

The variation of $(\beta - \alpha)$ along a diameter of a starch film can be calculated from the measured values of the acute axial angle $2V$ and the corresponding values of $(\gamma - \beta)$ (see the Supporting Information for more detail). Figure 6a shows the variation of $(\beta - \alpha)$ for the starch film (600 μL , 9.5 wt %) which is calculated from the measured values of $2V$ (see Figure 5b) and the values of $(\gamma - \beta)$ as shown in Figure 6a. It is found that although $(\gamma - \beta)$ varies considerably along the radial direction of the film, $(\beta - \alpha)$ remains almost constant.

The birefringence profiles of starch films obtained after drying droplets of the same volume but with different starch concentrations were measured to investigate the effects of the initial starch concentration. Figure 6b shows the $(\gamma - \beta)$ profiles of films obtained on drying 300 μL droplets with different starch concentrations. These profiles are plotted as a function of the normalized radial distance in the films. The profiles have similar characteristic variations with three different slopes along the radial direction. But the slope of the middle part of the birefringence profile tends to decrease on decreasing the initial starch concentration. The maximum values of birefringence near the edge of these films are close to each other, and hence it is independent of the initial starch concentration of droplets.

The birefringence profiles of the starch films formed after drying different volumes of droplets but with same initial starch concentration (6.5 wt %) were measured to study the effect of initial droplet volume. These profiles as a function of the normalized radial distance (r/r_0) are shown in Figure 6c. The superposition of all these data indicates that the effective birefringence $(\gamma - \beta)$ is a function of (r/r_0) only when the other experimental conditions remain the same. The very similar values of maximum birefringence near the edge of these films implies that it does not depend on the initial volume of the droplets.

The variation of index ellipsoid along the diameter of the starch film viewed from the top is schematically shown in the left side of Figure 7. The indicatrix in the biaxial region of the film is a general ellipsoid with three different principal indices α , β , and γ along the normal, radial, and azimuthal directions of the film, respectively. The intersection points between the optic axes and the ellipsoid in the biaxial region are indicated by a pair of black dots on each indicatrix in this diagram. The increasing angle $2V$ between the two optic axes toward the edge of the film widens the separation between these dots along the radially outward direction. At the center of the film and with uniaxial character, the index ellipsoid appears circular with the intersection point of the optic axis at its center. The right-hand side of Figure 7 shows the variation of index ellipse in the α - β plane along the diameter of the film. At the uniaxial center of the film, the birefringence is negative, and the index ellipsoid has an oblate shape. The indices α and β have maximum values at the center of the film, and they diminish monotonically toward the edge, keeping their difference almost equal.

The cryo-SEM studies of drying starch droplets were carried out to investigate the submicroscopic structures of the samples. Figures 8a,b show the cryo-SEM textures of a vertical cross-section of a droplet (300 μL , 9.5 wt %) 10 min after its dropcasting. The textures clearly show the presence of a thin solid crust on the free surface of the droplet (Figure 8a) and a cellular network inside the droplet (Figure 8b). It was found from cryo-SEM studies that the gelatinized starch samples after sonication consist of large numbers of nanoparticles of starch biopolymers. The solid crust forms due to the increased density of starch nanoparticles near the free surface of the droplet during its drying. The walls of the cellular structures are also composed of starch nanoparticles. Some of these nanoparticles are found to float inside these cells (see Figure S9 of the Supporting Information). The cellular network structure can account for the gelling property observed in our samples. A similar gel network structure has also been observed in the retrograded starch samples.^{48,49}

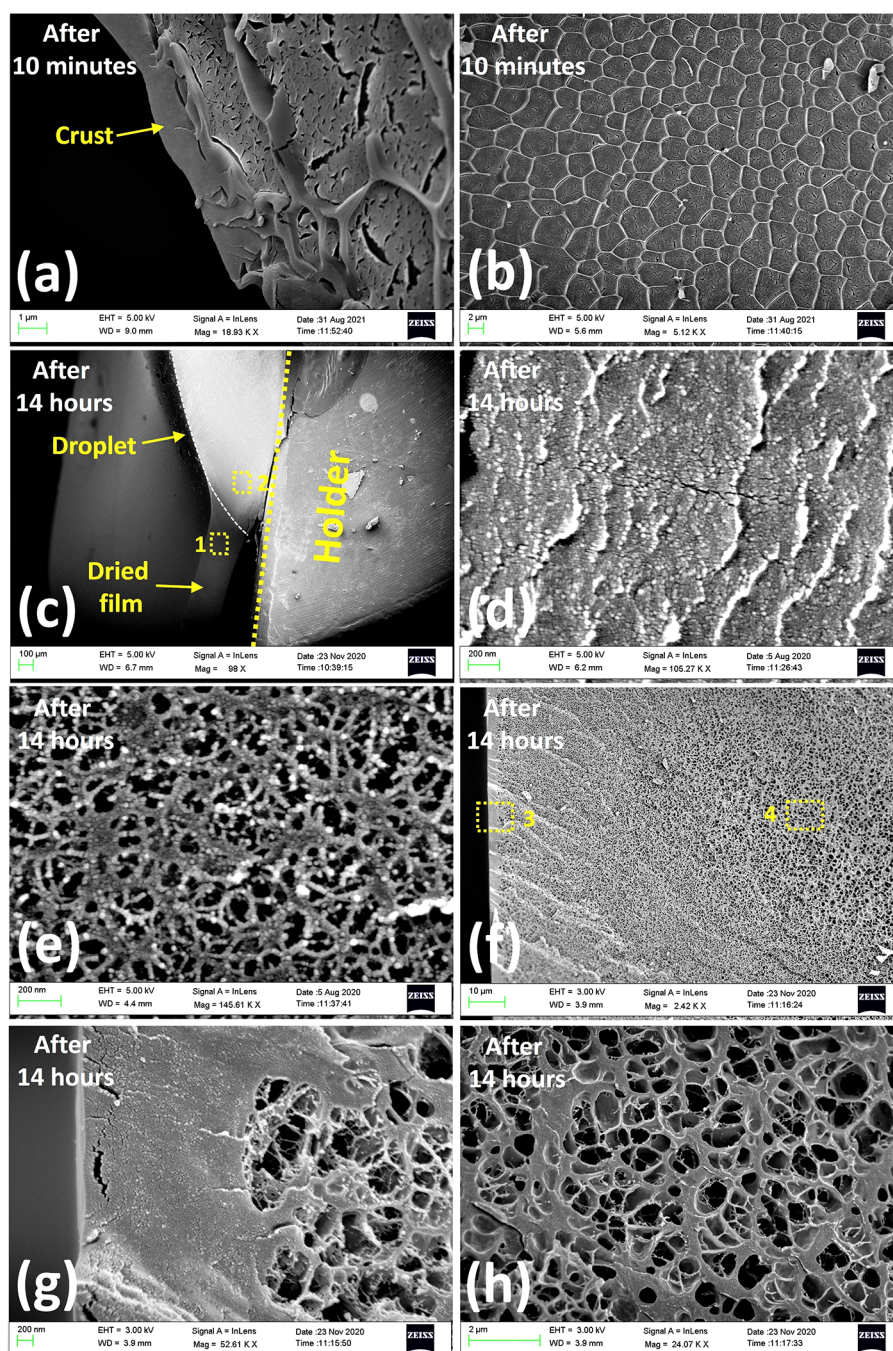


Figure 8. Cryo-SEM textures of the vertical cross-sections of droplets ($300\ \mu\text{L}$, 9.5 wt %) at different times after dropcasting. (a) The solid elastic crust on the surface of the droplet after 10 min. (b) The cellular network structure inside the droplet after 10 min. (c) The texture near the contact line after 14 h showing the droplet and the peripheral dried film fixed on the SEM holder. The magnified views of the marked region 1 (d) and region 2 (e) showing the texture of the dried starch film and the mesh structure inside the droplet, respectively. (f) The SEM texture near the central interfacial region of the droplet after 14 h. The magnified views of the marked region 3 (g) and region 4 (h) showing the crust on top of the droplet and the cellular network structure well inside the droplet, respectively.

The circular edge of the droplets ($300\ \mu\text{L}$, 9.5 wt %) after about 8 h starts to recede from the initial pinned edge toward the center, with the deposition of a peripheral film. Figure 8c shows the SEM texture of the vertical cross-section of such a droplet 14 h after dropcasting, near the receded contact line. The magnified views of regions marked 1 and 2 in this figure corresponding to the deposited film outside and the gel just inside the droplet edge are shown in Figure 8d and Figure 8e, respectively. It can be seen in Figure 8d that the deposited film is composed of densely packed starch nanoparticles. A mesh

structure made of starch nanoparticle filaments is observed in the magnified view of region 2 as shown in Figure 8e.

Figure 8f shows the cross-sectional cryo-SEM texture near the free surface at the central part of this droplet. Three different regions corresponding to a thin crust at the free surface, an intermediate mesh structure, and a core with a cellular structure have been observed in this part. A magnified view of the marked region 3 near the free surface is shown in Figure 8g, which depicts the dense crust at the free surface with the underlying mesh structure. The dense crust is formed by

densely packed starch nanoparticles and is the same as that found for the dried peripheral film shown in Figure 8d. The mesh region has a relatively large width but a lower density compared to that of the crust. The cellular network structure with the lowest density is observed below the mesh region. The magnified view of the marked region 4 of this cellular structure is shown in Figure 8h, which clearly reveals the membranes separating the cells. Therefore, it can be inferred from the SEM studies that the drying droplet develops a relatively thinner solid elastic crust at the free surface, an intermediate mesh region below the crust, and an inner core of a cellular network structure. The schematic diagrams of the drying starch droplet and its vertical cross-section showing these three regions are depicted in Figure 9. It is apparent that

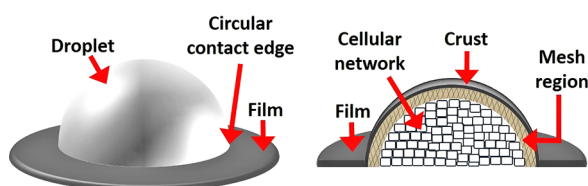


Figure 9. Schematic diagrams of the drying droplet and its vertical cross-section.

the cellular network structure gives rise to the denser mesh structure near the free surface of a droplet in the initial drying stages, which transforms to the dried film at the receding circular contact edge of the droplet upon further drying.

DISCUSSION

The coffee ring effect observed on drying polymeric solution droplets on flat substrates has been studied in detail.^{2,3,50} It was found that in a low concentration regime, the ring-like stain produced upon drying a droplet is due to the piling and deposition of the solute particles toward the edge, driven by capillary flow. This gives rise to a deposited film with a higher thickness at the edge compared to that at its center. Further studies showed that the difference in height at the edge and the center decreases with increasing polymer concentration.³ The deposited film becomes almost flat at a critical concentration. Upon further increase in the concentration, a dimple again starts to form near the center. The width and depth of the dimple in this high concentration regime increase with increasing polymer concentration. The flattening of the deposited film in the low concentration regime is thought to arise from the increasing viscosity of the solution on increasing the initial polymer concentration, which hinders the piling of solute toward the edge. However, the formation of the dimple in the high concentration regime is not well understood. It was conjectured that the dimple formation in the high concentration regime occurs due to the buckling of a crust of nonuniform thickness formed on the free surface of the droplet during its drying.³

In our sample, the cryo-SEM studies of drying droplets show a thin crust at the free surface of droplets, but the thickness of the crust is found to be uniform. We also found a mesh structure below the crust which is much thicker and denser toward the edge of the droplet compared to that near the top central region (see Figure S10 in the Supporting Information). We, however, have not observed the buckling of the crust during drying in our samples. Therefore, we propose the

following mechanism for the dimple formation on the starch films.

During drying, the droplet edge initially remains pinned to the substrate and subsequently starts to recede toward the center, depositing a peripheral film as shown in Figure 1. In our sample, a cellular network structure develops in the core in addition to the thin crust and the mesh structure around the droplet as shown in Figure 8. The deposited film, the crust, as well as the mesh structure have relatively higher densities compared to the core cellular network region. The deposition of this higher density peripheral film, therefore, generates a radially outward stress on the interior gel network structure during drying. This enhances the network density near the edge, creating a low density region near the center of the droplet. Hence on subsequent drying, a dimple forms at the central region of the deposited film.

We also have found that the dimple in starch films becomes deeper and wider on increasing the initial starch concentration (see Figure 2c and Figure 2d). The formation of the gel network structure in the droplet occurs earlier with increasing initial starch concentration. Therefore, the generated stress in the droplets with higher initial starch concentration becomes operative relatively earlier after dropcasting than in the droplets with lower initial concentration. These effects produce the dimple on the film deeper and wider with increasing initial starch concentration as observed in our experiments. The starch nanoparticles observed in our samples are expected to be birefringent due to the aggregated structure of the starch biopolymers. We propose that the alignment of these nanoparticles near the circular receding edge of the droplet during drying perhaps leads to the formation of birefringence in the deposited starch film.

CONCLUSION

The drying dynamics of droplets of gelatinized potato starch solutions on a flat substrate have been studied. The droplet is initially pinned to the substrate at its circular contact line. The edge of the droplet subsequently starts to recede toward the center, leaving a birefringent peripheral film from their initial pinned edge. The circular films formed after complete drying are azimuthally symmetric and show an “M-shaped” thickness profile along their diameter with a dimple at their center. The width and depth of the dimples in dried films increase by increasing the initial starch concentration. The cryo-SEM studies of a drying droplet show a cellular network structure at the core, an intermediate mesh region, and a solid crust of uniform thickness around the free surface of the droplet. The mesh structure is denser than the core cellular structure. Based on our experimental results, we propose that the dimple formation and the “M-shaped” thickness profile arise due to the evaporation-induced deposition of the film which produces a radially outward stress on the gel network structure in the drying droplet. This stress drags the network structure toward the edge, giving rise to a low density region at the center which subsequently forms a dimple at the center of the film upon complete drying. The POM studies show that the films at their center are optically uniaxial, with the optic axis perpendicular to the films, but become increasingly biaxial away from the center. The cryo-SEM studies also reveal that the microstructures of the droplet and the film are composed of starch nanoparticles which are possibly birefringent in nature. The orientational order of these nanoparticles near the receding edge of the droplet perhaps gives rise to the birefringence in

the deposited film. Further detailed experimental studies are required to confirm the origin of the birefringence of these films.

■ ASSOCIATED CONTENT

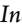
SI Supporting Information

The Supporting Information is available free of charge at <https://pubs.acs.org/doi/10.1021/acsomega.3c02164>.

The Supporting Information contains the detail about (a) the optical retardation measurement setup by using PEM and (b) the sample preparation for cryo-SEM studies, (c) the weight loss curve of a starch solution droplet (150 μL , 9.5 wt %) during its drying on a plastic substrate, (d) UV–visible transmission spectrum of a starch film, the derivation of the formulas for measuring (e) acute axial angle and (f) $(\beta - \alpha)$, (g) the conoscopic figures along the radial direction of a starch film (600 μL , 9.5 wt %), the cryo-SEM textures of vertical cross-section of starch solution droplets (300 μL , 9.5 wt %) after about (h) 10 min and (i) 14 h of their dropcasting. (ZIP)

■ AUTHOR INFORMATION

Corresponding Author

Arun Roy – Raman Research Institute, Bengaluru 560080, India;  orcid.org/0000-0003-4890-241X; Email: aroy@rri.res.in

Author

Subhadip Ghosh – Raman Research Institute, Bengaluru 560080, India

Complete contact information is available at:

<https://pubs.acs.org/doi/10.1021/acsomega.3c02164>

Notes

The authors declare no competing financial interest.

■ ACKNOWLEDGMENTS

We would like to thank Ms. Vasudha K. N. for her help in acquiring XRD data and UV–vis transmission spectra. We also would like to thank Mr. K. M. Yatheendran for his help in cryo-SEM imaging.

■ REFERENCES

- (1) Kajiya, T.; Kobayashi, W.; Okuzono, T.; Doi, M. Controlling the drying and film formation processes of polymer solution droplets with addition of small amount of surfactants. *J. Phys. Chem. B* **2009**, *113*, 15460–15466.
- (2) Kajiya, T.; Kaneko, D.; Doi, M. Dynamical visualization of “coffee stain phenomenon” in droplets of polymer solution via fluorescent microscopy. *Langmuir* **2008**, *24*, 12369–12374.
- (3) Kajiya, T.; Nishitani, E.; Yamaue, T.; Doi, M. Piling-to-buckling transition in the drying process of polymer solution drop on substrate having a large contact angle. *Phys. Rev. E* **2006**, *73*, 011601.
- (4) Smalyukh, I. I.; Zribi, O. V.; Butler, J. C.; Lavrentovich, O. D.; Wong, G. C. L. Structure and dynamics of liquid crystalline pattern formation in drying droplets of DNA. *Phys. Rev. Lett.* **2006**, *96*, 177801.
- (5) Maheshwari, S.; Zhang, L.; Zhu, Y.; Chang, H.-C. Coupling between precipitation and contact-line dynamics: multiring stains and stick-slip motion. *Phys. Rev. Lett.* **2008**, *100*, 044503.
- (6) Duggal, R.; Hussain, F.; Pasquali, M. Self-assembly of single-walled carbon nanotubes into a sheet by drop drying. *Adv. Mater.* **2006**, *18*, 29–34.
- (7) Zhang, S.; Li, Q.; Kinloch, I. A.; Windle, A. H. Ordering in a droplet of an aqueous suspension of single-wall carbon nanotubes on a solid substrate. *Langmuir* **2010**, *26*, 2107–2112.
- (8) Li, Q.; Zhu, Y. T.; Kinloch, I. A.; Windle, A. H. Self-organization of carbon nanotubes in evaporating droplets. *J. Phys. Chem. B* **2006**, *110*, 13926–13930.
- (9) Zhao, Y.; Cavallaro, G.; Lvov, Y. Orientation of charged clay nanotubes in evaporating droplet meniscus. *J. Colloid Interface Sci.* **2015**, *440*, 68–77.
- (10) Querner, C.; Fischbein, M. D.; Heiney, P. A.; Drndić, M. Millimeter-scale assembly of CdSe nanorods into smectic superstructures by solvent drying kinetics. *Adv. Mater.* **2008**, *20*, 2308–2314.
- (11) Martin, A.; Schopf, C.; Pescaglioni, A.; Wang, J. J.; Iacopino, D. Facile formation of ordered vertical arrays by droplet evaporation of Au nanorod organic solutions. *Langmuir* **2014**, *30*, 10206–10212.
- (12) Davidson, Z. S.; Huang, Y.; Gross, A.; Martinez, A.; Still, T.; Zhou, C.; Collings, P. J.; Kamien, R. D.; Yodh, A. Deposition and drying dynamics of liquid crystal droplets. *Nat. Commun.* **2017**, *8*, 1–7.
- (13) Chu, G.; Zussman, E. From chaos to order: evaporative assembly and collective behavior in drying liquid crystal droplets. *J. Phys. Chem. Lett.* **2018**, *9*, 4795–4801.
- (14) Deegan, R. D.; Bakajin, O.; Dupont, T. F.; Huber, G.; Nagel, S. R.; Witten, T. A. Capillary flow as the cause of ring stains from dried liquid drops. *Nature* **1997**, *389*, 827–829.
- (15) Deegan, R. D.; Bakajin, O.; Dupont, T. F.; Huber, G.; Nagel, S. R.; Witten, T. A. Contact line deposits in an evaporating drop. *Phys. Rev. E* **2000**, *62*, 756–765.
- (16) Parisse, F.; Allain, C. Drying of colloidal suspension droplets: experimental study and profile renormalization. *Langmuir* **1997**, *13*, 3598–3602.
- (17) Haw, M.; Gillie, M.; Poon, W. Effects of phase behavior on the drying of colloidal suspensions. *Langmuir* **2002**, *18*, 1626–1633.
- (18) Shi, J.; Yang, L.; Bain, C. D. Wetting and drying of aqueous droplets containing nonionic surfactants C_nE_m . *Langmuir* **2021**, *37*, 4091–4101.
- (19) Basu, N.; Mukherjee, R. Evaporative drying of sodium chloride solution droplet on a thermally controlled substrate. *J. Phys. Chem. B* **2020**, *124*, 1266–1274.
- (20) Choudhury, M. D.; Dutta, T.; Tarafdar, S. Pattern formation in droplets of starch gels containing NaCl dried on different surfaces. *Colloids Surf., A* **2013**, *432*, 110–118.
- (21) Brutin, D.; Sobac, B.; Loquet, B.; Sampil, J. Pattern formation in drying drops of blood. *Journal of fluid mechanics* **2011**, *667*, 85–95.
- (22) Gorr, H. M.; Zueger, J. M.; McAdams, D. R.; Barnard, J. A. Salt-induced pattern formation in evaporating droplets of lysozyme solutions. *Colloids Surf., B* **2013**, *103*, 59–66.
- (23) Pal, A.; Gope, A.; Athair, A. S.; Iannacchione, G. S. A comparative study of the drying evolution and dried morphology of two globular proteins in de-ionized water solutions. *RSC Adv.* **2020**, *10*, 16906–16916.
- (24) Yunker, P. J.; Still, T.; Lohr, M. A.; Yodh, A. Suppression of the coffee-ring effect by shape-dependent capillary interactions. *Nature* **2011**, *476*, 308–311.
- (25) Zang, D.; Tarafdar, S.; Tarasevich, Y. Y.; Dutta Choudhury, M.; Dutta, T. Evaporation of a Droplet: From physics to applications. *Phys. Rep.* **2019**, *804*, 1–56.
- (26) Lohani, D.; Basavaraj, M. G.; Satapathy, D. K.; Sarkar, S. Coupled effect of concentration, particle size and substrate morphology on the formation of coffee rings. *Colloids Surf., A* **2020**, *589*, 124387.
- (27) Pham, T.; Kumar, S. Drying of Droplets of Colloidal Suspensions on Rough Substrates. *Langmuir* **2017**, *33*, 10061–10076.
- (28) Beyer, S. T.; Walus, K. Controlled orientation and alignment in films of single-walled carbon nanotubes using inkjet printing. *Langmuir* **2012**, *28*, 8753–8759.

- (29) Pauchard, L.; Allain, C. Stable and unstable surface evolution during the drying of a polymer solution drop. *Phys. Rev. E* **2003**, *68*, 052801.
- (30) Pauchard, L.; Allain, C. Mechanical instability induced by complex liquid desiccation. *Comptes Rendus Physique* **2003**, *4*, 231–239.
- (31) Pauchard, L.; Allain, C. Buckling instability induced by polymer solution drying. *EPL (Europhysics Letters)* **2003**, *62*, 897.
- (32) Okuzono, T.; Ozawa, K.; Doi, M. Simple Model of Skin Formation Caused by Solvent Evaporation in Polymer Solutions. *Phys. Rev. Lett.* **2006**, *97*, 136103.
- (33) Maki, K. L.; Kumar, S. Fast Evaporation of Spreading Droplets of Colloidal Suspensions. *Langmuir* **2011**, *27*, 11347–11363.
- (34) Wang, S.; Copeland, L. Molecular disassembly of starch granules during gelatinization and its effect on starch digestibility: a review. *Food & function* **2013**, *4*, 1564–1580.
- (35) Kim, S.; Kang, J.-H.; Song, K. B. Development of a sword bean (*Canavalia gladiata*) starch film containing goji berry extract. *Food and Bioprocess Technology* **2020**, *13*, 911–921.
- (36) Nikvarz, N.; Khayati, G. R.; Sharafi, S. Bio-based ultraviolet protective packaging film preparation using starch with incorporated date palm syrup. *Mater. Chem. Phys.* **2021**, *270*, 124794.
- (37) Yun, D.; Cai, H.; Liu, Y.; Xiao, L.; Song, J.; Liu, J. Development of active and intelligent films based on cassava starch and chinese bayberry (*Myrica rubra* Sieb. et Zucc.) anthocyanins. *RSC Adv.* **2019**, *9*, 30905–30916.
- (38) Vieira, M. G. A.; da Silva, M. A.; dos Santos, L. O.; Beppu, M. M. Natural-based plasticizers and biopolymer films: A review. *European polymer journal* **2011**, *47*, 254–263.
- (39) Jenkins, P. J.; Donald, A. M. Gelatinisation of starch: a combined SAXS/WAXS/DSC and SANS study. *Carbohydr. Res.* **1998**, *308*, 133–147.
- (40) Liu, H.; Lelievre, J.; Ayoung-Chee, W. A study of starch gelatinization using differential scanning calorimetry, X-ray, and birefringence measurements. *Carbohydr. Res.* **1991**, *210*, 79–87.
- (41) Zhang, B.; Dhital, S.; Flanagan, B. M.; Gidley, M. J. Mechanism for starch granule ghost formation deduced from structural and enzyme digestion properties. *J. Agric. Food Chem.* **2014**, *62*, 760–771.
- (42) Debet, M. R.; Gidley, M. J. Why do gelatinized starch granules not dissolve completely? Roles for amylose, protein, and lipid in granule “ghost” integrity. *J. Agric. Food Chem.* **2007**, *55*, 4752–4760.
- (43) Jane, J.-L.; Wong, K.-S.; McPherson, A. E. Branch-structure difference in starches of A- and B-type X-ray patterns revealed by their Naegeli dextrans. *Carbohydr. Res.* **1997**, *300*, 219–227.
- (44) Cheetham, N. W.; Tao, L. Variation in crystalline type with amylose content in maize starch granules: an X-ray powder diffraction study. *Carbohydr. Polym.* **1998**, *36*, 277–284.
- (45) Domene-Lopez, D.; Garcia-Quesada, J. C.; Martin-Gullon, I.; Montalban, M. G. Influence of starch composition and molecular weight on physicochemical properties of biodegradable films. *Polymers* **2019**, *11*, 1084.
- (46) Imberty, A.; Perez, S. A revisit to the three-dimensional structure of B-type starch. *Biopolymers* **1988**, *27*, 1205–1221.
- (47) Pichler, H.; Schmitt-Riegraf, C. *Rock-forming Minerals in Thin Section*; Springer Netherlands: Dordrecht, 1997; pp 19–27.
- (48) Wu, Y.; Lin, Q.; Chen, Z.; Wu, W.; Xiao, H. Fractal analysis of the retrogradation of rice starch by digital image processing. *Journal of Food Engineering* **2012**, *109*, 182–187.
- (49) Utrilla-Coello, R.; Bello-Perez, L. A.; Vernon-Carter, E.; Rodriguez, E.; Alvarez-Ramirez, J. Microstructure of retrograded starch: quantification from lacunarity analysis of SEM micrographs. *Journal of Food Engineering* **2013**, *116*, 775–781.
- (50) Kajiya, T.; Monteux, C.; Narita, T.; Lequeux, F.; Doi, M. Contact-line recession leaving a macroscopic polymer film in the drying droplets of water-poly(N,N-dimethylacrylamide)(PDMA) solution. *Langmuir* **2009**, *25*, 6934–6939.